2026 IEEE/SICE International Symposium on System Integration (SII)
January 11-14, 2026. Cancún, México

# ANSI/RIA R15.08-1/2 and ANSI/A3 R15.08-2 Compliant Safety-Oriented Software Components for Industrial Mobile Robots

Samuel Kangwagye[1,2†], Mazin Hamad[1], Alessandro De Toni[1,3], Vasilije Rakčević[1], Valentin Le Mesle[1], Achim J. Lilienthal[1,4] and Sami Haddadin[1,5]

***Abstract*— Recent advancements in industrial robotics have led to the introduction of updated safety standards, including ANSI/RIA R15.08-1/2 and ANSI/A3 R15.08-2, which establish guidelines for Industrial Mobile Robots (IMRs). However, many aspects of these standards have not yet been explored in the context of IMR safety component development. This paper presents the design and integration of safety-oriented software components that align with these standards, with the goal of enhancing safety and efficiency of IMRs in intralogistics environments. We propose a multi-layer motion planning architecture, a planning and control framework for the manipulator, and a whole-body impedance controller that treats the IMR as a unified system. Additionally, we integrate components for robot intent communication, human perception, and human-robot spatial interaction to improve safety and user experience. Validation experiments in industrial settings demonstrate the effectiveness of the developed components in ensuring safe and adaptive IMR operation in shared and collaborative human-robot workspaces. The video demo can be seen at `https://youtu.be/Zmt_1h1CSlE`.**

## I. Introduction

In modern industrial environments, the demand for increased efficiency and flexibility has driven the adoption of robotics in diverse applications. However, many production processes, such as High-Mix Low-Volume (HVLM) manufacturing, still rely on human workers to handle complex tasks requiring adaptability and precision. As fully automated systems are often impractical for such settings, the focus has shifted to developing robotic systems capable of coexisting and collaborating with humans [1]. Robots must exhibit advanced capabilities to achieve smooth integration in human-robot co-production environments, including predictive planning, risk-aware motion strategies, and dynamic whole-body manipulation. For instance, learning and exploiting human activity patterns, predicting motions, and communicating intent are essential aspects to ensure safety and efficiency [2]. However, the increasing development of novel industrial robots with such capabilities continuously introduces new challenges for human-robot interaction (HRI) in industrial settings, as detailed in a recent survey [3]. Although the general goal is to achieve a high level of automation, many argue that collaboration between humans and robots is an unavoidable intermediate step. As a result, safety becomes a crucial aspect in the development of every robotic system [4]. Moreover, compared to fully automated production, having human-in-the-loop introduces additional challenges and requires introducing some safety margins [5], [6].

The first steps toward exploring the possibility of safe interaction in robotic manipulators were pioneered by foundational works such as [7], which experimentally analyzed robot-induced injuries and provided a better understanding of safe robot speeds for physical HRI (pHRI). Since then, collaborative robots, or cobots, have become integral to industrial processes, ranging from factory production to consumer-oriented applications [8]. However, ensuring physical safety alone might not be sufficient, as human perception and acceptance should also be considered. This led to the concept of *gracefully safe robots* introduced in [9]. The perceived safety and acceptance of a robotic system can be improved by the generation of 'human-like' motions [10] or visual cues, such as LED signals on the robot structure or in-the-floor projections [11]. Nonetheless, such features might be system-specific, and their integration into a wide range of mobile robots remains a challenge [12], [13]. Another approach contributing to the perceived safety is the addition of an Anthropomorphic Robotic Mock Driver (ARMoD) [14], which was employed to generate naturalistic cues such as gaze direction or arm gestures. Consequently, developing various safety-oriented components and continuous advancements in industrial robotics have posed the need for standardization. To address the challenges of pHRI and adopt a systematic approach to avoiding undesired and potentially dangerous situations, including harmful collisions, both updated and new standards, particularly for industrial robots, have been released. These include, for example, the international standards **ISO 10218-1/2** and the **ISO/TS 15066**[1], the American **ANSI/RIA R15.08-1/2** and **ANSI/A3 R15.08-2** for industrial robots [15]. Specifically, the novel aspect of the recent releases of these

This work was supported in part by the European Union's Horizon 2020 research and innovation programme as part of the project Darko under grant no. 101017274, in part by the Federal Ministry of Research, Technology and Space of Germany in the programme of "Souverän. Digital. Vernetzt.". Joint project 6G-life, project identification number: 16KISK002, in part by the Bavarian State Ministry for Economic Affairs, Regional Development and Energy (StMWi) for financial support as part of the project SafeRoBAY (grant number: DIK0203/01), in part by the Lighthouse Initiative Geriatronics by LongLeif GaPa gGmbH (Project Y), and in part by the Lighthouse Initiative KI.FABRIK Bayern by StMWi Bayern (grant no. DIK0249).

[1] Munich Institute of Robotics and Machine Intelligence (MIRMI), Technical University of Munich (TUM), 80992, Munich, Germany.

[2] Robotics and Automation Group, Department of Materials and Production, Aalborg University, 9220 Aalborg, Denmark.

[3] Department of Industrial Engineering (DIN), University of Bologna (UNIBO), 40126 Bologna, Italy.

[4] Mobile Robotics and Olfaction Lab, Center for Applied Autonomous Sensor Systems, Örebro University, Sweden.

[5] Mohamed bin Zayed University of Artificial Intelligence (MBZUAI), Masdar City, Abu Dhabi, United Arab Emirates

[†]Corresponding author. Email: `samkan@mp.aau.dk`

[1]The RIA TR R15.606 is the identical adoption provided by the American Robotic Industries Association (RIA) of ISO/TS 15066 as a technical report.

two standards is the introduction of guidelines for IMRs [15]. A first attempt of integrating a multi-layer safety-oriented navigation architecture has been proposed in [16]. However, that approach is limited to intra-logistic operations and was not assessed in light of the recently introduced **ANSI/RIA R15.08-1/2** IMR safety standard. Thus, aligning and verifying their safety components is still an open challenge.

The main contribution of this paper is the development and integration of novel safety-oriented components into an IMR platform for tasks involving both manipulation and mobile platform control at autonomous and interactive levels as shown in Fig. 1. These components are designed to align with selected sections of **ANSI/RIA R15.08-1/2** and **ANSI/A3 R15.08-2** standards. The scientific contributions of this paper are summarized as follows

- Requirements elicitation from the **ANSI/RIA R15.08-1/2** and **ANSI/A3 R15.08-2** standards regarding safety components of IMRs.
- Proposal and developments of safety-oriented software components in accordance with these standard requirements, as well as elaboration of their technical details.
- Validation of the effectiveness of integrating the developed components into an exemplary IMR[2] to ensure its safe operation around human workers in various realistic industrial settings.

The proposed safety components include a motion planning architecture, a planning and control framework for the arm only, and a whole-body impedance controller for the IMR system. For this, the manipulator and mobile base are treated as a unified system, enabling simultaneous operation of both subsystems. This approach improves efficiency and allows the IMR to exhibit whole-body compliance behavior during interactions with its environment. Other deployed components include an adaptation of the robot intent communication system, human perception stack, and human-robot spatial interaction (HRSI). For each of these components, the corresponding standards are highlighted. The integration of these components in the IMR is evaluated via a test scenario, which is a representation of the use case environment where workers and robots interact together. This paper focuses on the high-level design and integration of safety-oriented components in the IMR, their alignment with established standards, and their role in ensuring safety. Therefore, detailed mathematical formulations and analyses are not included.

## II. Considered Robot System and Safe Motion Unit

### A. IMR Hardware and Software Setup

The proposed safety-oriented components are integrated and tested on the IMR platform shown in Fig. 1. This IMR integrates an industrial omni-wheeled mobile vehicle, a Franka Emika Panda manipulator arm [18] on top, and a NAO mini-humanoid robot [19] as an ARMoD to form

[2]The considered IMR was manufactured by an industrial partner and further developed within the EU project DARKO on dynamic agile production robots for intralogistics applications [17].

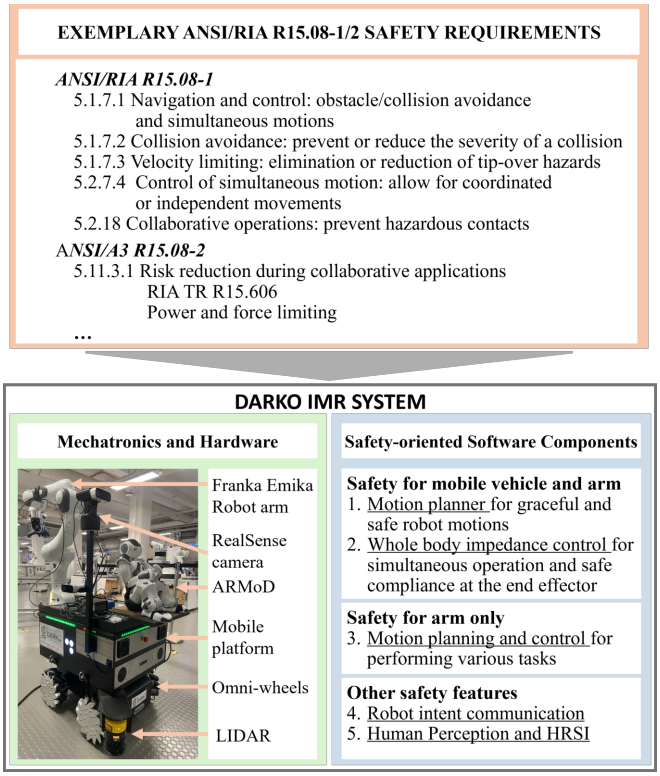


Fig. 1. The recent releases of the ANSI/RIA R15.08-1/2 introduce various requirements for IMR systems. This paper focuses on safety-oriented software components and their integration on an IMR, the DARKO platform, including a mobile platform, a Franka Emika Panda manipulator [18], and an Anthropomorphic Robotic Mock Driver (ARMoD) [14].

a combined mobile manipulator system with interaction capabilities. Efforts were placed to refine all the platform's features, ensuring compatibility with current developments and future requirements. The key novelties of this IMR are: 1) unlike conventional methods that treat the manipulator and base (mobile vehicle) as separate systems, the IMR in Fig. 1 is considered as a single, unified robot allowing simultaneous operation of the arm and mobile base, and 2) the NAO robot is added to the IMR to provide more communication channels (see Section III-D.1).

### B. Vehicle Safe Motion Unit (vSMU) Framework

A unified approach to ensuring human safety during pHRI with stationary robot arms involves an injury data-driven safety framework known as the Safe Motion Unit (SMU) [20]. This framework uses the human's relative position to the robot arm to impose speed limits, either in Cartesian space or at the joint level of the manipulator.

To this end, the SMU for a fixed robot arm is modified and implemented on the mobile IMR system in Fig. 1, thus, the naming is modified to vehicle SMU (vSMU). A detailed procedural description of vSMU algorithm can be found in [21]. Here, the vSMU sets the limit for robot maximum speed based on the observed relative human-robot distance and their velocity information. Correlation between the motion speed and safety is based on a rich injury database for various impact curvatures - the vSMU shapes the robot motion such that the impact energy of possible dynamic collisions will not

lead to serious injury in the worst case. It is worth mentioning that the deployment of the vSMU requires considering the IMR as a unified system. This aspect and its impact on the controller is detailed further in Section III-B.

Another simplification considered for the safety unit is that the mobile vehicle is modeled as a floating base. Indeed, this is a valid simplification for the used platform since it accommodates omni-wheel drives characterized by holonomic motion.

*vSMU Operation Modes:* Safety operational modes can be generally distinguished as [22]: *autonomous* - no shared workspace, *coexistence* - human and the robot share the workspace but do not have a shared task purpose, *cooperation* - coexistance with a shared task purpose, and *collaboration* - cooperation that allows contact between the human partner and the robot. In this paper, the focus is set on autonomous, coexistance, and cooperation modes since the platform is treated as a single, unified robot. This can be seen as a simplification due to the rather different approach for safety in collaboration where the focus is on velocities of individual parts. To this end, considering a unified robot, the following situations are considered:
*Case 1*: Robot and human are moving towards each other.
*Case 2*: Both are moving in the same direction with the robot being behind the human and moving faster.
*Case 3*: Both are moving in the same direction but the human is behind the robot.

Regarding *Case 1*, the relative speeds are taken into consideration, otherwise the derived injury metric would not be valid. This approach has been introduced as a trade-off between safety and task execution efficiency. For *Case 2*, vSMU is expected to actively control the maximum speed of the robot: For the metric, it is rather that the absolute speeds are used (robot not taking advantage of additional speed margin available due to the human going away). For *Case 3*, it is expected that humans will not try to intentionally cause the collision with the robot. Thus, relative task velocity stays unaltered while the direction stays consistent.

## III. Proposed Safety-Oriented Components

### A. Motion Planning Architecture

In order to align with **ANSI/RIA R15.08-1-2020:5.1.7.1,2,3** and **ANSI/A3 R15.08-2-2023: 5.6.8**, a system needs to handle different contextual cues of the environment, static and dynamic ones, by generating natural, smooth, legible and safe robot motion. To achieve this, a motion planning architecture is developed based on the following requirements:

- Make use of the several *contextual cues* that the IMR can perceive. In particular, the planners are developed to handle the output generated by scene understanding and HRSI components presented in Section III-D.2.
- Plan considering different *time-scales and representations*. Contextual cues and human' dynamics are represented on different time scales. Usually, the semantics of the environments are reported in semi-static representations: maps that encode objects' semantics, which are updated while the robot is fulfilling its tasks. Humans' dynamics are often handled according to two different time scales: semi-static representations where long-term human motion patterns are reported (e.g., Maps of Dynamics (MoDs) [23], [24]), dynamic and punctual ones where the current and short-term predicted behaviors are detailed (e.g., trajectory predictions).
- Consider *risk and safety aspects* when planning the robot operation and motion. The generated plans should reduce the risk of collision or in general robot unsafe operation at a minimum.

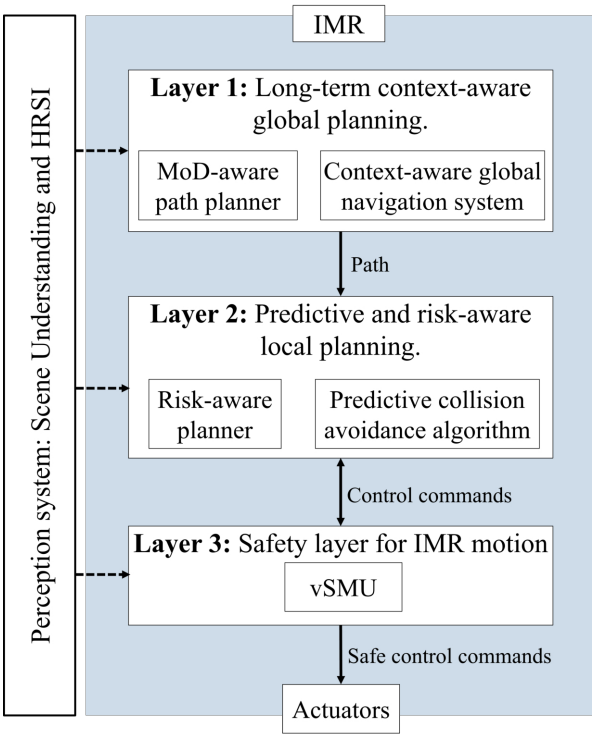


Fig. 2. Motion planning architecture composed of three main layers. Each layer handles different contextual aspects of the environment.

To this end, we consider the multi-layer motion planner introduced in [25] and depicted in Fig. 2, which follows a *predictive planning* setup: differently from a traditional *sense-plan-act* one [26], this architecture integrates predictions of surrounding humans and dynamic objects inside the different layers. This architecture is composed of three main layers:

**Layer 1: Long-term context-aware global planning**. This layer is responsible for generating paths for legible robot operations considering long-term human behaviors and semantics[3] of the environment.The desired path is generated by two components. First, a context-aware global planner enables reaching goals in partially unknown semantically-rich environments, bridging exploration with goal-directed navigation, considering primarily the static context. Then, a MoD-aware path planner handles the dynamic long-term context for navigation in human environments, represented with MoDs.

[3]Semantics can be represented as labeled data i.e., text labels associated to geometric entities and positions, or as neural network architecture embeds.

**Layer 2: Predictive and risk-aware local planning**. The paths computed in the first layer are then forwarded to the predictive and risk-aware local planning layer, which runs at a higher frequency (circa 20 Hz). Here, the paths are adapted according to different definitions of risk and by performing obstacle avoidance considering short-term predictions. First, the waypoints obtained in Layer 1 are processed by a risk-aware planner, which updates the path based on the probability of short-term collision and localization error. Then, a predictive collision avoidance algorithm generates the control commands, considering short-term predictions of nearby humans' behavior.

**Layer 3: Safety layer for IMR motion**. This layer, for which the implementation is the main focus of this paper, is responsible for the reshaping of computed velocity commands to meet safety requirements. To reduce the hazards and harms to surrounding humans, the velocities of the IMR are scaled based on bio-mechanical analysis of possible injuries to nearby people. The safety components used in this layer are described in Section II-B.

### *B. Whole Body Impedance Controller for the IMR*

Ensuring safe physical human-robot interactions requires the ability to achieve compliant behavior, as, in principle, the human could interact with any part of the robot. This section introduces an impedance controller that considers both the arm and the base as an integrated whole-body system, in accordance with **ANSI/RIA R15.08-1-2020: 5.1.7.1,2,4**. First, a unified whole-body dynamic model is constructed for the analysis of dynamics and kinematics. To construct a whole-body control system, a unified dynamic model that accounts for the coupling terms of inertia, Coriolis, and centrifugal torque is developed as

$$\begin{bmatrix} \boldsymbol{M}_v + \boldsymbol{M}_{a,up} & \boldsymbol{M}_{va} \\ \boldsymbol{M}_{va}^T & \boldsymbol{M}_a \end{bmatrix} \begin{bmatrix} \ddot{\boldsymbol{q}}_v \\ \ddot{\boldsymbol{q}}_a \end{bmatrix} + \begin{bmatrix} \boldsymbol{C}_v & \boldsymbol{C}_{va} \\ \boldsymbol{C}_{av} & \boldsymbol{C}_a \end{bmatrix} \begin{bmatrix} \dot{\boldsymbol{q}}_v \\ \dot{\boldsymbol{q}}_a \end{bmatrix} + \begin{bmatrix} \boldsymbol{0} \\ \boldsymbol{g}_a \end{bmatrix} = \begin{bmatrix} \boldsymbol{E}_v(\boldsymbol{q}_v)\boldsymbol{\tau}_v \\ \boldsymbol{\tau}_a \end{bmatrix} + \begin{bmatrix} \boldsymbol{\tau}_v^{\text{ext}} \\ \boldsymbol{\tau}_a^{\text{ext}} \end{bmatrix}, \tag{1}$$

where $\boldsymbol{q}_v \in \mathbb{R}^{n_{q_v}}$ and $\boldsymbol{q}_a \in \mathbb{R}^{n_{q_a}}$ are the vehicle available direction of motions and the arm joint variables. $\boldsymbol{M}_{va} \in \mathbb{R}^{n_{q_a} \times n_{q_v}}$ presents the inertial coupling between the mobile platform and the manipulator, capturing the influence of the platform's dynamics on the arm, $\boldsymbol{M}_{av} = \boldsymbol{M}_{va}^{\mathsf{T}} \in \mathbb{R}^{n_{q_v} \times n_{q_a}}$ describes the reciprocal dynamic effect of the manipulator on the mobile base. $\boldsymbol{C}_{av} \in \mathbb{R}^{n_{q_a}}$ represents Coriolis and centrifugal terms caused by the angular motion of the mobile base, $\boldsymbol{C}_{va} \in \mathbb{R}^{n_{q_v}}$ denotes Coriolis and centrifugal terms due to the presence of the manipulator, $\boldsymbol{M}_{v,up}$ accounts for the extra inertial effects arising from the arm being mounted on the base, $\boldsymbol{E}_v \in \mathbb{R}^{n_{q_v} \times n_{q_v}}$ is the input transformation matrix, $\boldsymbol{\tau}_v \in \mathbb{R}^{n_{q_v}}$ and $\boldsymbol{\tau}_a \in \mathbb{R}^{n_{q_a}}$ are the vehicle and arm control torques, $\boldsymbol{\tau}_v^{ext} \in \mathbb{R}^{n_{q_v}}$ and $\boldsymbol{\tau}_a^{ext} \in \mathbb{R}^{n_{q_a}}$ represent the contributes of external forces felt at joint level.

Additionally, obtaining a whole-body Jacobian matrix is crucial, as it allows to simultaneously account for the contributions of both the base and the arm movements to the end-effector's velocity. The calculation of the whole-body Jacobian matrix is as follows:

$$\begin{aligned} \begin{bmatrix} {}^{\mathbb{S}}\boldsymbol{v}_e \\ {}^{\mathbb{S}}\boldsymbol{\omega}_e \end{bmatrix} &= \begin{bmatrix} \boldsymbol{I}_{3\times3} & -{}^{\mathbb{S}}\boldsymbol{p}_{ve} \\ \boldsymbol{0}_{3\times3} & \boldsymbol{I}_{3\times3} \end{bmatrix} \begin{bmatrix} {}^{\mathbb{S}}\boldsymbol{v}_v \\ {}^{\mathbb{S}}\boldsymbol{\omega}_v \end{bmatrix} + \begin{bmatrix} {}^{\mathbb{S}}_{A}\boldsymbol{R} & \boldsymbol{0}_{3\times3} \\ \boldsymbol{0}_{3\times3} & {}^{\mathbb{S}}_{A}\boldsymbol{R} \end{bmatrix} \begin{bmatrix} {}^{\mathbb{A}}\boldsymbol{v}_{e,a} \\ {}^{\mathbb{A}}\boldsymbol{\omega}_{e,a} \end{bmatrix} \\ &= \begin{bmatrix} \boldsymbol{V}_v(\boldsymbol{q}_a){}^{\mathbb{S}}\boldsymbol{J}_v & \boldsymbol{V}_a(\boldsymbol{q}_v){}^{\mathbb{S}}\boldsymbol{J}_a(\boldsymbol{q}_a) \end{bmatrix} \begin{bmatrix} \boldsymbol{q}_v \\ \boldsymbol{q}_a \end{bmatrix}, \end{aligned} \tag{2}$$

where $\boldsymbol{I}_{3\times3}$ is the identity matrix, $\mathbb{S}$ and $A$ represent, respectively, the world frame and the manipulator's base frame, $\boldsymbol{v} \in \mathbb{R}^3$ and $\boldsymbol{\omega} \in \mathbb{R}^3$ are the translational and angular velocities of the entities described by the following subscripts: $e$ for end-effector, $v$ for vehicle, $e, a$ for end-effector velocity considering only arm contribute, ${}^{\mathbb{S}}\boldsymbol{p}_{ve} \in \mathbb{R}^3$ represents the translational displacement from the geometric center of the vehicle to the end-effector, ${}^{\mathbb{S}}_{A}\boldsymbol{R} \in \mathbb{R}^{3\times3}$ is the rotation matrix that transforms coordinates from $A$ to $\mathbb{S}$, ${}^{\mathbb{S}}\boldsymbol{J}_v \in \mathbb{R}^{6\times n_{q_v}}$ and ${}^{\mathbb{S}}\boldsymbol{J}_a \in \mathbb{R}^{6\times n_{q_a}}$ are, respectively, the vehicle and the arm Jacobian. Eventually,

$$\boldsymbol{V}_v(\boldsymbol{q}_a) = \begin{bmatrix} \boldsymbol{I}_{3\times3} & -{}^{\mathbb{S}}\boldsymbol{p}_{ve} \\ \boldsymbol{0}_{3\times3} & \boldsymbol{I}_{3\times3} \end{bmatrix} \text{ and } \boldsymbol{V}_a(\boldsymbol{q}_v) = \begin{bmatrix} {}^{\mathbb{S}}_{A}\boldsymbol{R} & \boldsymbol{0}_{3\times3} \\ \boldsymbol{0}_{3\times3} & {}^{\mathbb{S}}_{A}\boldsymbol{R} \end{bmatrix}.$$

To this end, the whole-body geometric Jacobian is formulated from (2) as

$${}^{\mathbb{S}}\boldsymbol{J} = \begin{bmatrix} \boldsymbol{V}_v(\boldsymbol{q}_a){}^{\mathbb{S}}\boldsymbol{J}_v & \boldsymbol{V}_a(\boldsymbol{q}_v){}^{\mathbb{S}}\boldsymbol{J}_a(\boldsymbol{q}_a) \end{bmatrix}. \tag{3}$$

Eventually, the whole-body Impedance control law is obtained by involving the whole-body dynamic and kinematic parameters in (1) and (3) and applying the Cartesian impedance controller presented in [27] to the whole system

$$\boldsymbol{\tau} = \boldsymbol{J}(\boldsymbol{q})^{\mathsf{T}}\boldsymbol{F}_{\boldsymbol{\tau}} = \boldsymbol{g}(\boldsymbol{q}) + \boldsymbol{J}(\boldsymbol{q})^{\mathsf{T}}\Big(\boldsymbol{\Lambda}(\boldsymbol{x})\ddot{\boldsymbol{x}}_d + \boldsymbol{\mu}(\boldsymbol{x}, \dot{\boldsymbol{x}})\dot{\boldsymbol{x}}_d - \boldsymbol{K}_d\widetilde{\boldsymbol{x}} - \boldsymbol{D}_d(\boldsymbol{x})\dot{\widetilde{\boldsymbol{x}}}\Big), \tag{4}$$

where $\widetilde{\boldsymbol{x}} = \boldsymbol{x} - \boldsymbol{x}_d$, with $\widetilde{\boldsymbol{x}} \in \mathbb{R}^6$, is the pose error, $\boldsymbol{\Lambda}(\boldsymbol{x}) \in \mathbb{R}^{6\times6}$ and $\boldsymbol{\mu}(\boldsymbol{x}, \dot{\boldsymbol{x}}) \in \mathbb{R}^{6\times6}$ are the inertial and Coriolis/centrifugal matrix in Cartesian space obtained from the joint space dynamical model (1) as explained in [28], $\boldsymbol{\tau} = \begin{bmatrix} \boldsymbol{\tau}_v & \boldsymbol{\tau}_a \end{bmatrix}^T \in \mathbb{R}^{n_{q_v}+n_{q_a}}$ is the whole-body control torque, $\boldsymbol{q} = \begin{bmatrix} \boldsymbol{q}_v & \boldsymbol{q}_a \end{bmatrix}^T \in \mathbb{R}^{n_{q_v}+n_{q_a}}$ are the whole-body joint positions, while $\boldsymbol{K}_d \in \mathbb{R}^{6\times6}$ ad $\boldsymbol{D}_d(\boldsymbol{x}) \in \mathbb{R}^{6\times6}$ are, respectively, the desired stiffness and damping matrix. After applying this impedance controller to the dynamic system in (1), the desired compliance behaviour to the external force is acquired as given below

$$\boldsymbol{f}_{\text{ext}} = \boldsymbol{\Lambda}(\boldsymbol{x})\ddot{\widetilde{\boldsymbol{x}}} + \Big(\boldsymbol{\mu}(\boldsymbol{x}, \dot{\boldsymbol{x}}) + \boldsymbol{D}_d(\boldsymbol{x})\Big)\dot{\widetilde{\boldsymbol{x}}} + \boldsymbol{K}_d\widetilde{\boldsymbol{x}}. \tag{5}$$

It is worth noting that the closed-loop system retains its original inertia as inertia shaping would require direct measurement of external forces at the end-effector level. This is a crucial choice for human-robot interaction since it allows to react to contacts that are detected anywhere on the robot structure by relying on joint torque sensing rather than being limited to interactions occurring solely at the end-effector.

Another important aspect to consider is that the mobile base can not be torque-controlled. As a consequence, a common

solution is to employ an admittance interface that emulates the impedance behavior commanded by (4), e.g. [29] as

$$\boldsymbol{M}_{adm}\ddot{\boldsymbol{q}}_v^{ref} + \boldsymbol{D}_{adm}\dot{\boldsymbol{q}}_v^{ref} = \boldsymbol{\tau}_v + \boldsymbol{\tau}_v^{ext}, \tag{6}$$

where $\boldsymbol{M}_{adm} \in \mathbb{R}^{n_{q_v} \times n_{q_v}}$ and $\boldsymbol{D}_{adm} \in \mathbb{R}^{n_{q_v} \times n_{q_v}}$ are the selected inertia and damping matrices for attaining the desired admittance, while $\dot{\boldsymbol{q}}_v^{ref}$ is the reference velocity obtained by plugging the control torque $\boldsymbol{\tau}_v$ in to the equation. In the absence of torque sensing at the base, the external torque acting on the vehicle $\boldsymbol{\tau}_v^{ext}$ is assumed to be zero and is treated as a disturbance. In this way it is not possible to detect contacts that happen at the mobile base.

The selection of impedance (or admittance) parameters presents a significant challenge, as they must simultaneously enforce the desired compliance, ensure satisfactory trajectory tracking performance, and maintain stability in contact-rich environments. One approach to simplifying this problem is to decouple the system dynamics in (1) by assuming quasi-static base movements [30] or employing feedback linearization techniques [29]. However, such modifications effectively obscure the true system dynamics. While this abstraction is generally acceptable for nominal operations, it may be insufficient for contact reactions, as physical interactions occur at a much higher frequency than the typical control update rates of impedance-based strategies. Nevertheless, in typical applications of IMRs, such as intralogistics, achieving high levels of whole-body dexterity is seldom required. As a result, decoupling manipulation tasks from locomotion does not significantly compromise performance. Therefore, treating the IMR as a whole-body system and addressing the associated challenges fall outside the scope of this work.

### C. Planning and Control Framework for Manipulator

As discussed in the latter part of Section III-B, by assuming quasi-static movements of the mobile base or explicitly decoupling locomotion tasks from manipulation tasks, it is possible to separately treat the arm and the mobile base from planning and control perspective. Based on these assumptions, a planning and control framework, that considers only the dynamics of the robotic arm, is presented. Consequently, since the dynamics of the IMR have been decoupled, here the safety framework has been reverted from vSMU to SMU.

*1) Low-level Control Algorithm:* Similar to the approach outlined in Section III-B, the control law chosen to follow a Cartesian reference is a classical Cartesian impedance controller [27], which ensures a safer interaction with the environment in comparison to the classical position controllers. Given a desired Cartesian trajectory $x_{des}$ and its time derivative $\dot{x}_{des}$, the error between the actual and desired Cartesian position and the velocity of the manipulator can be defined as $\boldsymbol{e} = \boldsymbol{x}_{\mathrm{des}} - \boldsymbol{x}$ and $\dot{\boldsymbol{e}} = \dot{\boldsymbol{x}}_{\mathrm{des}} - \dot{\boldsymbol{x}}$. From these values, the joint torque required to follow the desired trajectory can be computed as

$$\boldsymbol{\tau}_a = \boldsymbol{J}_a^{\mathsf{T}}(\boldsymbol{q}_a)(\boldsymbol{K}_p\boldsymbol{e} + \boldsymbol{K}_v\dot{\boldsymbol{e}}) + \boldsymbol{g}_a(\boldsymbol{q}_a) + \boldsymbol{C}_a(\boldsymbol{q}_a, \dot{\boldsymbol{q}}_a)\dot{\boldsymbol{q}}_a, \tag{7}$$

where $\boldsymbol{K}_p \in \mathbb{R}^{n_{q_a} \times n_{q_a}}$ and $\boldsymbol{K}_v \in \mathbb{R}^{n_{q_a} \times n_{q_a}}$ are matrices that define the impedance behavior of the controller, while the other terms have been defined in Section III-B. Running on a low-level controller means that the SMU does not distinguish between automatic and semi-automatic modes, aligning with **ANSI/A3 R15.08-2-2023: 5.8.2.2** standard.

*2) Human-Like Motion Planning:* Controlling the robot motions as human-like trajectories is essential for improving the motion's predictability and acceptance in human-robot interaction [31]. Thus, we implement the manipulator motion planning algorithm presented in [10], which relies on the functional Principal Component Analysis (fPCA) to represent human motion features with a smaller set of functional elements.

Thus, the desired planned trajectory is given by

$$x(t) = \bar{x} + S_0(t) + \sum_{i=1}^{5} \alpha_i S_i(t), \tag{8}$$

where $\bar{x}$ is the average pose of the hand, $S_0(t)$ is the average trajectory across all the trajectories in the dataset, $\alpha_i$ is a vector of weights, and $S_i(t)$ is the $i^{th}$ basis element. The details of computing the trajectory in (8) can be found in [10].

*3) Integration of planning and control framework with SMU:* The SMU sets the highest safe speed to prevent serious injuries in case of a collision with a human. Therefore, the motion planning algorithm must adjust the robot's movements to stay within the speed limits defined by the SMU. To achieve this, this paper proposes to use the SMU as a bridge between the Planner and the Controller where the Planner continuously calculates the maximum safe speed based on the robot's current position and human-related data. Here, only the manipulator's end effector is considered the Point of Interest, and the speed is limited based on the robot's reflected mass at that point. Since the system is built within the ROS framework, a publisher/subscriber setup is used to send the velocity limit from the SMU to the motion planning node. The SMU calculates the safe speed using the robot's current state and position relative to the worker, then shares this information through a dedicated topic.

On the motion planning side, the system continuously checks whether the planned speed follows the SMU constraint. If the speed is too high, it slows down the trajectory. From a technical perspective, the planning node runs in cycles, publishing each trajectory frame at the correct sampling time to ensure smooth motion. At each cycle, it receives the maximum safe speed from the SMU, compares it with the desired speed, and adjusts the sampling time to keep the motion within safety limits.

### D. Additional Deployed Safety-Oriented Components

*1) Robot Intent Communication System:* The interaction between a robotic system and a human user, especially if not specifically trained, is an important factor of perceived safety. Therefore, the ARMoD [14] can be placed onto the IMR platform and provides additional communication channels

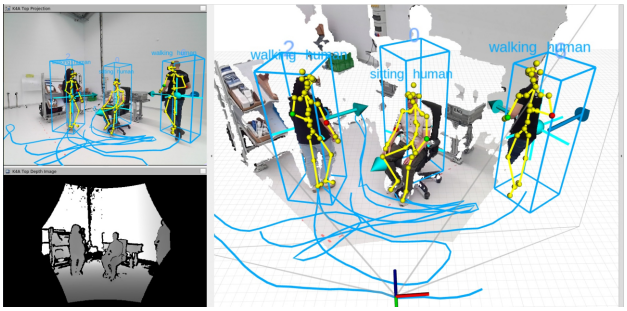


Fig. 3. Visualization of the integrated human perception stack that was deployed on Fig. 1. A single Azure Kinect RGB-D camera was used for human perception, its color and depth images are shown on the left. Bounding boxes have a fixed scale and indicate tracked persons, trailing blue lines their past trajectories, blue arrows their velocity vector. Cyan crosses represent oriented 3D centroids from the RGB-D YOLO detector.

such as A: Head for robotic gaze, B: Text-to-Speech engine for dialogues, C: Additional LEDs i.e., on the ARMoD torso, D: Arms for pointing, and other gestures. These features can improve the perceived safety and align with the **ANSI/A3 R15.08-2-2023: 5.2** standard.

*2) Human Perception and Human Robot Spatial Interaction Modules:* For the perception of humans around the robot using its onboard sensors, a modular perception pipeline developed in [32] was benchmarked. This aligns with **ANSI/A3 R15.08-2-2023: 5.11.3.1**. An example scene with a visualization of outputs from the 3D human perception stack deployed on Fig. 1 is shown in Fig 3. For HRSI, the risk evaluation approach studied in [33], [34] was employed to provide human intention predictions for the IMR.

## IV. Experiments and Results

### A. Validation of the Integrated System

The integration of the proposed safety-oriented components, introduced in Section III, in the IMR is evaluated in a selected use case scenario where the system is performing a pre-defined task while workers can freely approach the robot. The ARMoD is excluded here since it was previously tested in [14]. All parts of the system being ROS-compatible, the incoming data can be visualized in soft real-time using RViz, as shown in Fig. 4. As visualized in the virtual environment (top), worker classification (dangerous or safe) is indicated above its representation (red or green, respectively) and is determined based on the detected human position. The figure also displays the real environment and the virtual safety zones (bottom).

The robot is set to move between two positions in Cartesian space, emulating a task execution. The human worker is being perceived and his position, i.e., skeleton fit, orientation, speed, etc., is correctly localized in the environment, as well as with respect to the robot position. As the human enters the pre-configured safety zone, the vSMU is triggered to limit the robot's speed. As can be seen in Fig. 5, the speed reduction ratio is computed in the online control cycle and is not a constant value - it is a result of a comparison of the robot's current speed with the maximum safe speed at the current robot position, depending on the robot's perceived environment data. The video demo can be seen at `https://youtu.be/Zmt_1h1CS1E`.

### B. Integration of the Human-like Motion Planner

A second integration experiment, between the human-like motion planner and the SMU, is then conducted. In this test, the mobile platform remains at a fixed location and the planner is asked to move the manipulator's end-effector forward and backward along the same trajectory on the horizontal plane. At time $t = 5$s, a human comes in front of the manipulator, activating the SMU. The obtained end-effector Cartesian velocities are presented in Fig. 6. It can be observed that the presence of a human near the manipulator, depicted as colored areas, leads to a decrease in the end-effector Cartesian velocity. Another interesting thing to note is that the decrease is stronger when the x component of the velocity is positive. This happens because when $v_x > 0$, the end-effector is moving toward the human and the SMU sets a lower maximum allowed velocity to limit dangerous collision.

## V. Conclusions

This paper presented the integration of safety-oriented software components into an IMR system, ensuring compliance with the latest ANSI/RIA R15.08-1/2 and ANSI/A3 R15.08-2 safety standards. The proposed components were incorporated into a multi-layer motion planning framework, addressing both long-term and short-term safety considerations. To enhance physical safety, we introduced whole-body impedance controllers, both for the overall IMR system and specifically for the manipulator arm, enabling adaptive compliance in dynamic environments. Our experimental validation demonstrated that the IMR and the manipulator arm effectively adjusts their velocity in response to human presence, leveraging the (v)SMU safety framework to minimize potential risks. Additionally, we examined the role of perceived safety by integrating components for robot intent communication and spatial interaction with humans, further aligning with the defined safety guidelines.

The results highlight the feasibility of implementing safety-oriented software components to improve IMR safety and interaction in industrial settings. Future work will focus on extending the validation to more complex scenarios and refining the adaptability of the safety framework to diverse industrial environments.

## References

[1] A. Hentout, M. Aouache, A. Maoudj, and I. Akli, "Human–robot interaction in industrial collaborative robotics: a literature review of the decade 2008–2017," *Advanced Robotics*, vol. 33, no. 15-16, pp. 764–799, 2019.

[2] S. Haddadin, A. De Luca, and A. Albu-Schäffer, "Robot collisions: A survey on detection, isolation, and identification," *IEEE Transactions on Robotics*, vol. 33, no. 6, pp. 1292–1312, 2017.

[3] W. Li, Y. Hu, Y. Zhou, and D. T. Pham, "Safe human–robot collaboration for industrial settings: a survey," *Journal of Intelligent Manufacturing*, vol. 35, no. 5, pp. 2235–2261, 2024.

[4] J. Guiochet, M. Machin, and H. Waeselynck, "Safety-critical advanced robots: A survey," *Robotics and Autonomous Systems*, vol. 94, pp. 43–52, 2017.

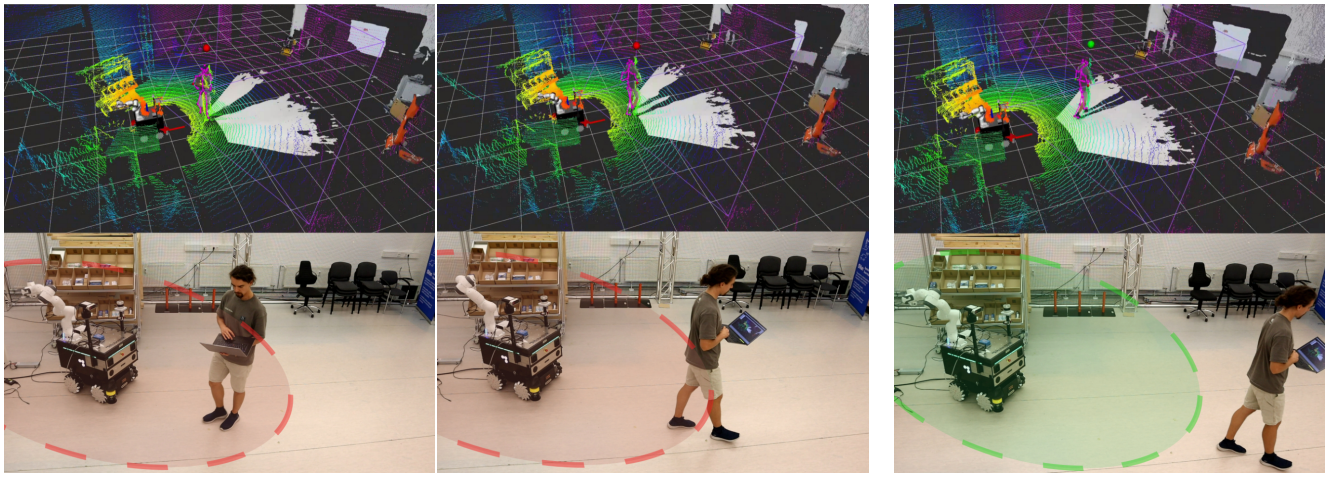

Fig. 4. Captures of the RViz visualization (top) and camera recording (bottom) of the integrated system experiment. The presence of a human in a non-safe area (left - red area) is detected by the safety-oriented software component and is visualized by a red dot in RViz. In this case, the velocity of the IMR is adapted. Likewise, a human detected in a safe area (right) is represented by a green dot on RViz.

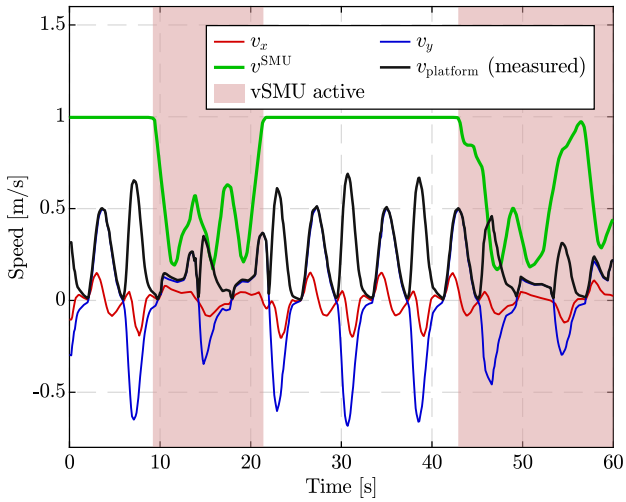


Fig. 5. Recorded data velocities alongside the safety velocity value. The colored region refers to the time when the vSMU is triggered by the presence of a human in an unsafe region.

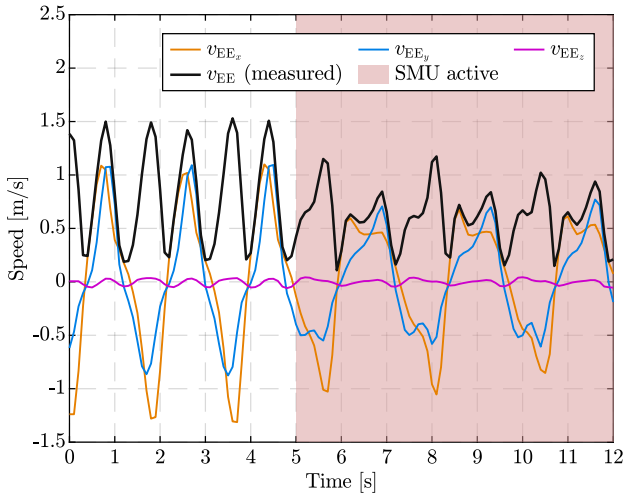


Fig. 6. Velocity profiles obtained during the second integration test, between human-like motion planner and SMU. From $t = 5$s, represented as the colored area, a human goes in front of the manipulator, activating the SMU velocity scaling.


[5] M. Bdiwi, M. Pfeifer, and A. Sterzing, "A new strategy for ensuring human safety during various levels of interaction with industrial robots," *CIRP Annals*, vol. 66, no. 1, pp. 453–456, 2017.

[6] A. Zacharaki, I. Kostavelis, A. Gasteratos, and I. Dokas, "Safety bounds in human robot interaction: A survey," *Safety science*, vol. 127, p. 104667, 2020.

[7] S. Haddadin, A. Albu-Schaffer, M. Frommberger, J. Rossmann, and G. Hirzinger, "The dlr crash report: Towards a standard crash-testing protocol for robot safety - part i: Results," in *Proceedings - IEEE International Conference on Robotics and Automation*, 06 2009, pp. 272 – 279.

[8] F. Vicentini, "Collaborative robotics: a survey," *Journal of Mechanical Design*, vol. 143, no. 4, 2021.

[9] M. Hamad, S. Nertinger, R. J. Kirschner, L. Figueredo, A. Naceri, and S. Haddadin, "A concise overview of safety aspects in human-robot interaction," in *Human-Friendly Robotics 2023*, C. Piazza, P. Capsi-Morales, L. Figueredo, M. Keppler, and H. Schütze, Eds. Cham: Springer Nature Switzerland, 2024, pp. 1–18.

[10] M. Baracca, G. Averta, and M. Bianchi, "A general approach for generating artificial human-like motions from functional components of human upper limb movements," *Control Engineering Practice*, vol. 148, p. 105968, 2024. [Online]. Available: https://www.sciencedirect.com/science/article/pii/S096706612400128X

[11] R. T. Chadalavada, H. Andreasson, M. Schindler, R. Palm, and A. J. Lilienthal, "Bi-directional navigation intent communication using spatial augmented reality and eye-tracking glasses for improved safety in human–robot interaction," *Robotics and Computer-Integrated Manufacturing*, vol. 61, p. 101830, 2020.

[12] E. Cha, Y. Kim, T. Fong, M. J. Mataric *et al.*, "A survey of nonverbal signaling methods for non-humanoid robots," *Foundations and Trends® in Robotics*, vol. 6, no. 4, pp. 211–323, 2018.

[13] G. Angelopoulos, F. Vigni, A. Rossi, G. Russo, M. Turco, and S. Rossi, "Familiar acoustic cues for legible service robots," in *2022 31st IEEE International Conference on Robot and Human Interactive Communication (RO-MAN)*. IEEE, 2022, pp. 1187–1192.

[14] T. Schreiter, L. Morillo-Mendez, R. T. Chadalavada, A. Rudenko, E. Billing, M. Magnusson, K. O. Arras, and A. J. Lilienthal, "Advantages of Multimodal versus Verbal-Only Robot-to-Human Communication with an Anthropomorphic Robotic Mock Driver," in *2023 32nd IEEE International Conference on Robot and Human Interactive Communication (RO-MAN)*. IEEE, 2023, pp. 293–300.

[15] American National Standards Institute and Robotic Industries Association (RIA) and its parent company Association for Advancing Automation (AAA), "ANSI/RIA R15.08-1:2020 - American National Standard for Industrial Mobile Robots Safety Requirements - Part 1: Requirements for the Industrial Mobile Robot," 2021.

[16] S. Molina, A. Mannucci, M. Magnusson, D. Adolfsson, H. Andreasson, M. Hamad, S. Abdolshah, R. T. Chadalavada, L. Palmieri, T. Linder, C. S. Swaminathan, T. P. Kucner, M. Hanheide, M. Fernandez-Carmona, G. Cielniak, T. Duckett, F. Pecora, S. Bokesand, K. O. Arras,

S. Haddadin, and A. J. Lilienthal, "The iliad safety stack: Human-aware infrastructure-free navigation of industrial mobile robots," *IEEE Robotics & Automation Magazine*, vol. 31, no. 3, pp. 48–59, 2024.

[17] DARKO consortium, "Initial DARKO mobile dynamic manipulation platform," Deliverable 1.1, EU project DARKO, Tech. Rep., 2018.

[18] S. Haddadin, "The franka emika robot: A standard platform in robotics research," *IEEE Robotics & Automation Magazine*, 2024.

[19] D. Gouaillier, V. Hugel, P. Blazevic, C. Kilner, J. Monceaux, P. Lafourcade, B. Marnier, J. Serre, and B. Maisonnier, "The nao humanoid: a combination of performance and affordability," *arXiv preprint arXiv:0807.3223*, 2008.

[20] S. Haddadin, S. Haddadin, A. Khoury, T. Rokahr, S. Parusel, R. Burgkart, A. Bicchi, and A. Albu-Schäffer, "A truly safely moving robot has to know what injury it may cause," in *2012 IEEE/RSJ International Conference on Intelligent Robots and Systems*, 2012, pp. 5406–5413.

[21] M. Hamad, A. Kurdas, N. Mansfeld, S. Abdolshah, and S. Haddadin, "Modularize-and-conquer: A generalized impact dynamics and safe precollision control framework for floating-base tree-like robots," *IEEE Transactions on Robotics*, vol. 39, no. 4, pp. 3200–3221, 2023.

[22] P. Svarny, M. Hamad, A. Kurdas, M. Hoffmann, S. Abdolshah, and S. Haddadin, "Functional mode switching for safe and efficient human-robot interaction," in *2022 IEEE-RAS 21st International Conference on Humanoid Robots (Humanoids)*, 2022, pp. 888–894.

[23] T. P. Kucner, M. Magnusson, E. Schaffernicht, V. H. Bennetts, and A. J. Lilienthal, "Enabling flow awareness for mobile robots in partially observable environments," *IEEE Robotics and Automation Letters (RA-L)*, vol. 2, no. 2, pp. 1093–1100, Apr. 2017.

[24] T. P. Kucner, M. Magnusson, S. Mghames, L. Palmieri, F. Verdoja, C. S. Swaminathan, T. Krajník, E. Schaffernicht, N. Bellotto, M. Hanheide *et al.*, "Survey of maps of dynamics for mobile robots," *The International Journal of Robotics Research*, p. 02783649231190428.

[25] E. Stracca, A. Rudenko, L. Palmieri, P. Salaris, L. Castri, N. Mazzi, V. Rakcevic, N. Vaskevicius, T. Linder, N. Belloo, T. Schreiter, Y. Zhu, M. Castellano Quero, O. Napolitano, E. Stefanini, L. Heuer, M. Magnusson, A. Swikir, and A. J. Lilienthal, "Darko-nav, hierarchical risk- and context-aware robot navigation in complex intralogistic environments," in *European Robotics Forum (ERF)*, 2025.

[26] B. Siciliano, O. Khatib, and T. Kröger, *Springer handbook of robotics*. Springer, 2008, vol. 200.

[27] C. Ott, "Cartesian impedance control: The rigid body case," *Cartesian Impedance Control of Redundant and Flexible-Joint Robots*, pp. 29–44, 2008.

[28] O. Khatib, "A unified approach for motion and force control of robot manipulators: The operational space formulation," *IEEE Journal on Robotics and Automation*, vol. 3, no. 1, pp. 43–53, 1987.

[29] A. Dietrich, K. Bussmann, F. Petit, P. Kotyczka, C. Ott, B. Lohmann, and A. Albu-Schäffer, "Whole-body impedance control of wheeled mobile manipulators: Stability analysis and experiments on the humanoid robot rollin'justin," *Autonomous Robots*, vol. 40, pp. 505–517, 2016.

[30] Y. Wu, P. Balatti, M. Lorenzini, F. Zhao, W. Kim, and A. Ajoudani, "A teleoperation interface for loco-manipulation control of mobile collaborative robotic assistant," *IEEE Robotics and Automation Letters*, vol. 4, no. 4, pp. 3593–3600, 2019.

[31] A. M. Zanchettin, L. Bascetta, and P. Rocco, "Acceptability of robotic manipulators in shared working environments through human-like redundancy resolution," *Applied ergonomics*, vol. 44, no. 6, pp. 982–989, 2013.

[32] T. Linder, N. Vaskevicius, R. Schirmer, and K. O. Arras, "Cross-modal analysis of human detection for robotics: An industrial case study," in *IEEE/RSJ International Conference on Intelligent Robots and Systems (IROS)*, 2021.

[33] L. Castri, S. Mghames, M. Hanheide, and N. Bellotto, "Causal discovery of dynamic models for predicting human spatial interactions," in *International Conference on Social Robotics*. Springer, 2022, pp. 154–164.

[34] ——, "Enhancing causal discovery from robot sensor data in dynamic scenarios," in *Conference on Causal Learning and Reasoning*, vol. 213. PMLR, 2023, pp. 243–258.